An effective temperature calibration for main-sequence B- to F-type stars using $VJHK_\mathrm{s}$ colors

Ernst Paunzen[1], Martin Netopil[1], and Andreas Herdin[2]
[1] Department of Theoretical Physics and Astrophysics, Masaryk University, Kotlářská 2, 611 37 Brno, Czech Republic
[2] Universitätssternwarte, Türkenschanzstr. 17, 1180 Wien, Austria
epaunzen@physics.muni.cz
(Submitted on 29.08.2016. Accepted on 12.09.2016)

Abstract. The effective temperature is an important parameter that is needed for numerous astrophysical studies, in particular to place stars in the Hertzsprung-Russell diagram, for example. Although the availability of large spectroscopic surveys increased significantly in the last decade, photometric data are still much more frequent. Homogeneous photometric (all-sky) surveys provide the basis to derive the effective temperature with reasonable accuracy also for objects that are not covered by spectroscopic surveys, or are out of range for the current spectroscopic instrumentations because of too faint magnitudes. We use data of the Two Micron All Sky Survey (2MASS) and broadband visual photometric measurements to derive effective temperature calibrations for the intrinsic colors $(V-J)$, $(V-H)$, $(V-K_\mathrm{s})$, and $(J-K_\mathrm{s})$, valid for B2 to F9 stars. The effective temperature calibrations are tied to the Strömgren-Crawford $uvby\beta$ photometric system and do not depend on metallicity or rotational velocity.
Key words: stars: early-type – stars: fundamental parameters – techniques: photometric

Introduction

With the development of high quality and stable astronomical infrared array technology, between 1997 and 2001, the Two Micron All Sky Survey (2MASS) provided a full-sky census with millijansky sensitivity and arcsecond resolution (Skrutskie et al., 2006). It presented precise photometry and astrometry over the entire celestial sphere in the J (1.25 μm), H (1.65 μm), and K_s (2.16 μm) bands. In total, almost 471 000 000 point and 1 650 000 extended sources were observed.

The scientific output of this survey had an important impact on almost all fields of astrophysics. For example the study of the coolest low-mass stars (Geißler et al., 2011), the investigation of the large-scale metallicity distribution in the Galactic bulge (Gonzalez et al., 2013), and the compilation of a galaxy group catalog (Tully, 2015), just to mention a few.

One of the most basic and important diagnostic diagrams when it comes to stellar astrophysical parameters is still the Hertzsprung-Russell diagram (HRD; Hertzsprung, 1911; Russell, 1913). Originally, the spectral type and the absolute magnitude were used to describe the evolutionary status of an object. Nowadays, we are able to measure the absolute magnitudes (or luminosities) of stars very precisely thanks to space based satellite missions such as Hipparcos (Perryman et al., 1997) and Gaia (Perryman, 2005). However, still an estimate of the total absorption (reddening) in the line-of-sight is needed to derive them. For this, reddening maps (Schlafly et al., 2014) or secondary calibrations (Reis et al., 2011) can be used. Instead of the spectral types, mostly the colors or effective temperatures of stars are used. This has several reasons. First of all, the efforts to derive classification for stars are either based on photographic plates (Houk & Swift, 1999) or are limited to interesting fields on the sky, such as the one observed by the Kepler satellite (De Cat et al., 2015). In addition, still the classical spectral classification (MKK) scheme by Morgan et al. (1943) is widely used. However, especially for B- to F-type stars, some efforts were spent (Garrison & Gray, 1994) to include the effects of rotation and metallicity on the spectral classification. Another severe limitation is the shift of the current available spectroscopic instruments to the red optical and infrared region, but the MKK scheme is defined for the spectral region from 3800 Å to about 4700 Å. For stars hotter than G0, there are almost no useable metallic lines in the red regime (Torres-Dodgen & Weaver, 1993).

Colors and their effective temperature calibration were discovered as being a powerful extension or substitution of the spectral types by the introduction of well defined broad and narrow-band photometric systems together with the usage of photomultipliers. One of the most successful and powerful astronomical photometric system is the $uvby\beta$ one, introduced by Bengt Strömgren (Strömgren, 1956) and extended by David Crawford (Crawford, 1958). It was mainly designed to investigate stars and their basic astrophysical characteristics in an accurate way. It measures the effective temperature, the Balmer discontinuity, and blanketing due to metallic lines. Furthermore, it can be used to estimate the interstellar reddening. Several reddening-free indexes for many different purposes and spectral type regions have been developed so far (Fiorucci & Munari, 2003). The Geneva-Copenhagen Survey of the Solar Neighborhood (Holmberg et al., 2009), for example, includes a magnitude-complete, kinematically unbiased sample of 16 682 nearby F and G dwarfs and is the largest available sample with complete data for stars with ages spanning that of the disk. It is still the most used and reliable photometric system when it comes to determine the effective temperature and reddening of stars over the complete spectral region.

Coming back to the NIR region, several heuristic effective temperature calibrations have been published in the past (Fernley, 1989; di Benedetto, 1998; Masana et al., 2006; Worthey & Lee, 2011). Most of the published calibrations concentrate on stars cooler than F-type.

In this paper, we present a new effective temperature calibration that is tied to the $uvby\beta$ system using $VJHK_{\mathrm{s}}$ colors of normal B- to F-type main-sequence, i.e. between or close the zero- and terminal-age-main-sequence (ZAMS and TAMS) stars. For this, precise parallax data from Hipparcos and the available photometry (Kharchenko, 2001; Skrutskie et al., 2006) were used. The goal is to establish a calibration which is not influenced by the rotational velocity and metallicity of the target stars.

The final calibration is based on highly accurate data of 523 stars in the given spectral type region. A comparison with recent published intrinsic colors of stars was done and a good agreement has been found. Furthermore, we analyzed possible offsets and correlations due to high rotational velocities and metallicities different than solar.

Naturally, the calibration can be applied as well to any photometric data that is tied to the 2MASS system, such as the UKIRT Infrared Deep Sky Survey (Lawrence et al., 2007). It is quite evident that the use of photo-

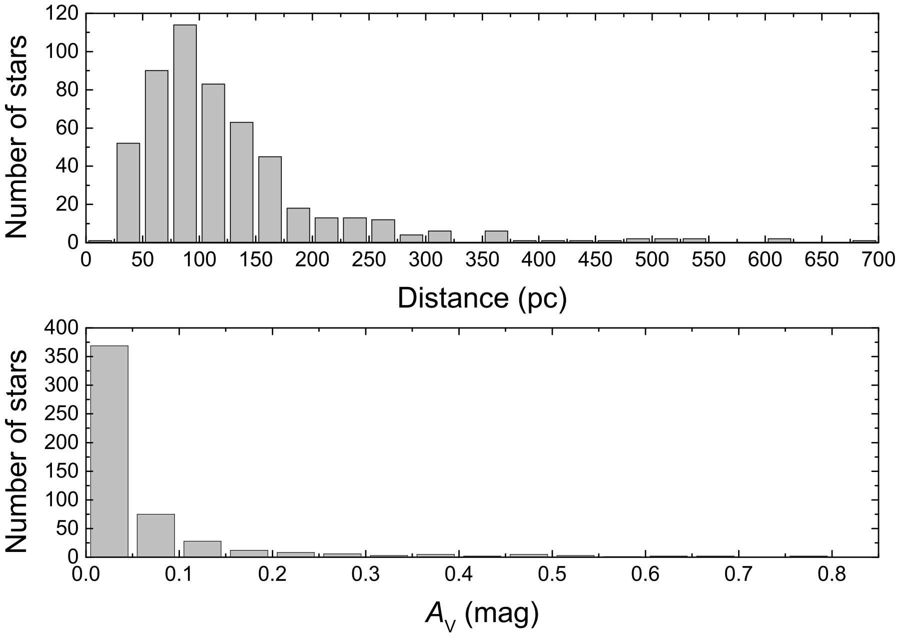

Fig. 1. The distributions of the distance and total absorption of our sample.

metric colors which include the V-band are beneficial, because of the wider color range. Numerous open clusters or field stars are already covered in this photometric band, the data can be queried from ongoing surveys, such as the AAVSO Photometric All-Sky Survey (APASS[3]), or can be transformed from *ugriz* colors (Jordi et al., 2006). The calibration can be used, for example, to statistically derive the metallicities of open clusters (Pöhnl & Paunzen, 2010; Netopil & Paunzen, 2013) or for an automatic pipeline software for already available or forthcoming surveys.

Finally, two widely different applications are presented. First, the temperatures of well-established chemically peculiar stars of the upper main sequence were calibrated and compared with the results by Netopil et al. (2008). In addition, the effective temperatures derived for 117 A- and F-type stars from the Kepler field on the basis of high-resolution spectroscopy (Niemczura et al., 2015) were used to test our calibration. The comparisons result in an excellent agreement showing the capabilities of the presented calibration.

[3] http://www.aavso.org/apass

Target selection

For our statistical analysis we needed a homogeneous sample of main sequence stars for which accurate astrometric, photometric, and spectroscopic data exist. First, we searched for all entries in the Hipparcos catalog (van Leeuwen, 2007) which satisfy the adopted error range of the parallaxes ($\sigma_\pi / \pi \leq 12.5\%$). The latter limit was chosen such as not to introduce a significant error due to the Lutz-Kelker effect (Lutz & Kelker, 1973) for a sample chosen by parallaxes only (see next discussion in the next Section). For the chosen limit, the maximum correction for the absolute magnitude is 0.18 mag which is in the range of the expected error from all other error sources. The $uvby\beta$ photometry data were taken from Hauck & Mermilliod (1998), the NIR photometry data from 2MASS (Skrutskie et al., 2006), and additional visual photometric data from the All-Sky Compiled Catalogue of 2.5 million stars (ASCC; Kharchenko, 2001) and the General Catalogue of Photometric data (GCPD[4]). If the catalogs contained more than one measurement of a photometric index of a star, we used its mean value. As next step, the sample was restricted to a 1-σ error of the broad band photometric measurements to $\sigma_\lambda \leq 0.1$ mag for $VJHK_\mathrm{s}$. Furthermore, the 1-σ errors of the small band photometric indexes were constrained as follows: $\beta = (b-y) \leq 0.027$ mag, $m_1 \leq 0.032$ mag, and $c_1 \leq 0.050$ mag following the suggestion by Balona (1994). The spectral types for these objects were extracted from the extensive list by Skiff (2009 – 2016). All B- to F-type stars with luminosity classes from I to III were excluded whereas luminosity class IV were a priori not eliminated. This is because the luminosity classes V and IV can not be clearly separated in the HRD (Paunzen, 1999). Therefore, our sample should only include hydrogen-burning stars. As final step, all objects which are listed as variable, chemically peculiar, or are in binary systems were removed by cross matching with the GCVS database (Samus et al., 2007 – 2016), the General Catalogue of Ap and Am stars (Renson & Manfroid, 2009), and the Hipparcos catalog (Perryman et al., 1997). Finally, 523 normal type stars remain with high quality data according to the above listed standards.

The stars are not homogeneously distributed over the spectral type range. There are 131 (25%) B-, 127 (24%) A-, and 265 (51%) F-type stars included.

Figure 1 (upper panel) shows the histogram of the distances directly calculated from the parallaxes. Almost all stars are within 300 pc around the Sun. The more distant stars are all B-type objects because the relative error (used as a selection criterion) directly scales with the apparent and therefore the absolute magnitude (van Leeuwen & Fantino, 2005).

Analysis

For the final goal, to derive a calibration of the effective temperature in terms of the different colors, and to locate the stars in the HRD, two additional observational parameters needed to be determined, first. These are

[4] http://gcpd.physics.muni.cz/

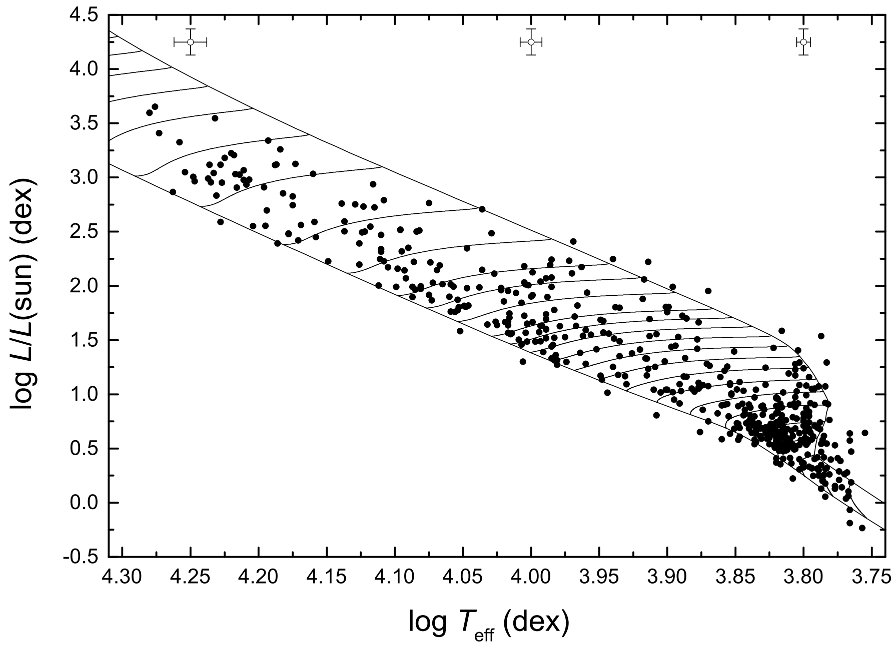

Fig. 2. The HRD of our targets with the stellar tracks taken from Bressan et al. (2012). ZAMS and TAMS and lines of equal masses from 1 to 8 $M_\odot$ are included. In the upper part of the diagram, the maximum error bars are given.

the total absorption A_V (reddening) and the bolometric correction (B.C.). For the latter, the values from Flower (1996) were applied. This reference is still the most widely used one and was tested countless times for many different objects (Buzzoni et al., 2010).

The reddening estimation in the $uvby\beta$ photometric system is based on the comparison of the reddened $(b-y)$ and c_1 with the unreddened $(u-b)$ and β indexes for B-type stars (Crawford, 1978). For cooler stars, the reddening is estimated by the standard relations of the different indexes using the values given by Hilditch et al. (1983); Schuster & Nissen (1989); Domingo & Figueras (1999).

For the B-type stars, we compared the reddening estimates with those derived from the Q method in the UBV photometric system (Johnson, 1958) which yielded an excellent agreement. One has to keep in mind that these stars are the most distant ones with a high reddening, probably also because of their youth and location in star forming regions with a significant amount of dust as well as gas around them.

For the dereddening of the $VJHK_s$ magnitudes, we used the following reddening ratios for the different filters (Dutra et al., 2002):

$$E(b-y) = 0.24A(V) = 0.07A(J) = 0.04A(H) = 0.03A(K_s) \tag{1}$$

In Figure 1 (lower panel), the distribution of the total absorption is shown for our target sample. Because of the close distance to the Sun, more than 2/3 of the stars exhibit $A_{\rm V} \leq 0.05$ mag.

To get the effective temperatures of our program stars, we used the most widely used calibration by Napiwotzki et al. (1993). It was tested countless times and found to be still, the most homogeneous one for the $uvby\beta$ system. Basically, the calibration is divided into three regions: 1) for stars hotter than 11 000 K, the unreddened $[u-b]$ and c_0 colors; 2) objects between 11 000 K and 8 500 K, the a_0 and r^* indexes; and 3) for cooler stars the β index are applied. The derived effective temperature values were independently checked in two different ways. First of all, we made use of the SED fitting tool by Robitaille et al. (2007). As input data, the available photometry together with the distances and reddening values were taken. In addition, the effective temperature calibrations covering B- to mid F-type stars within the Johnson UBV system (if available) listed by Paunzen et al. (2005, 2006) were applied. For none of our targets, a significant deviating value was found. This means that the available photometry in the different systems is intrinsically consistent. The final sample consists of stars with $3.75 < \log T_{\rm eff} < 4.30$ dex. The upper limit does not cover stars hotter and more massive than B2V due to the lack of precise parallax measurements of such objects.

As a next step, the HRD of the target sample was constructed. Using the parallax, reddening, and apparent magnitude (V) of each object, we calculated the absolute magnitude ($M_{\rm V}$). With the individual B.C., the absolute bolometric magnitude $M_{\rm Bol} = M_{\rm V} + B.C.$ and, finally, with the absolute bolometric magnitude of the Sun (4.74 mag), the luminosity $\log L/L_{\odot}$ was derived. To calculate the error of this parameter, let us recall the propagation of uncertainties for the luminosity estimation. Applying the equation for the variance of a function of several variables, we get:

$$\sigma(M_{\rm V}) = \sqrt{\left(\tfrac{2.17}{\pi}\right)^2 \sigma(\pi)^2 + \sigma(V)^2 + \sigma(A_{\rm V})^2} \tag{2}$$

$$\sigma(\log L/L_{\odot}) = \tfrac{\sigma(M_{\rm Bol})}{2.5} \tag{3}$$

By far, the largest contribution is the uncertainty of the parallax. Our choice of $\sigma_{\pi}/\pi \leq 12.5\%$ transforms into $\sigma(\log L/L_{\odot}) \leq 0.11$ dex. Another error source is the so-called Lutz-Kelker effect (Lutz & Kelker, 1973). They were among the first to calculate corrections for the bias in the absolute magnitude of a star as estimated from its trigonometric parallax. The bias is introduced by ubiquitous random errors of measurements which, on average, cause the trigonometric parallax to be overestimated. The correction reaches 0.43 mag for $\sigma_{\pi}/\pi = 17.5\%$. However, since the publication of the Hipparcos data, there is an ongoing debate if this effect should be considered for single stars or not. Recently, Francis (2014) showed, on the basis of Monte-Carlo simulations that the overall correction for the absolute magnitude can be described as

$$\mathit{\Delta}(M_{\rm V}) = -5.35 \left(\frac{\sigma(\pi)}{\pi}\right)^2 . \tag{4}$$

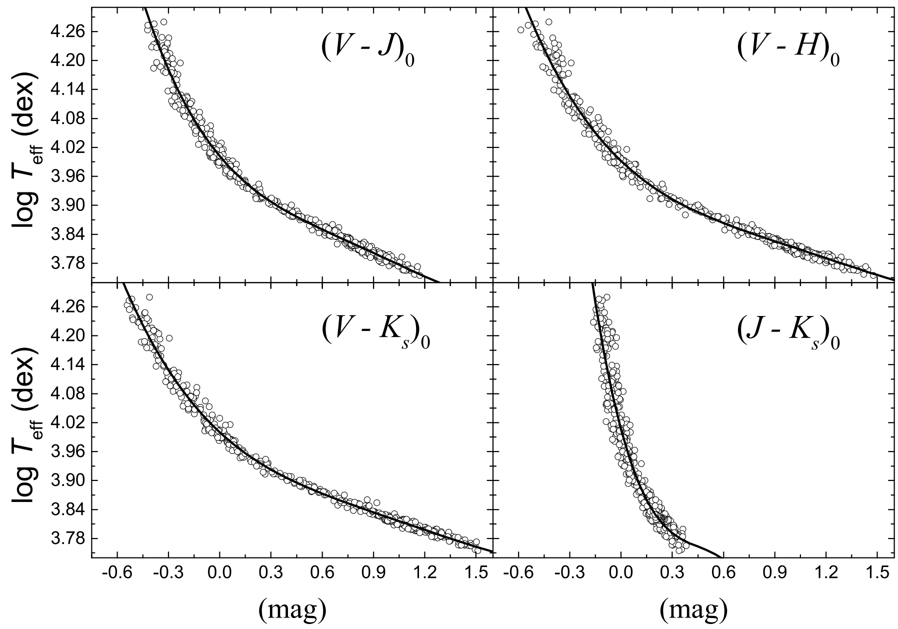

Fig. 3. The dereddened colors versus the $\log T_{\mathrm{eff}}$ diagrams for our 523 targets.

For our given accuracy limit this transforms to $\sigma(\log L/L_{\odot}) \leq 0.03$ dex as the maximum deviation. This is a factor of about four smaller than the contribution of the parallax error.

Figure 2 shows the location of our target stars in the HRD. The stellar tracks and isochrones of the PAdova and TRieste Stellar Evolution Code v1.2s (PARSEC; Bressan et al., 2012) with Z = 0.017 and Y = 0.279 were used as a reference frame. It is clearly visible that all stars are, within the errors, between the ZAMS and TAMS with masses between 8 and 1 $\mathrm{M}_{\odot}$ (spectral types B2 to F9/G0). As already expected from the spectral types, the stars are not homogeneously distributed over the whole mass and luminosity range. We conclude that all chosen objects are hydrogen burning stars of luminosity classed V and IV.

For the final calibrations, we have chosen the following color indexes: $(V-J)_0$, $(V-H)_0$, $(V-K_{\mathrm{s}})_0$, and $(J-K_{\mathrm{s}})_0$. To select the degree of the appropriate polynomial regression, the cross-validation method (Breaz, 2004) was applied. Basically, it minimizes the expected prediction error by varying the polynomial degree. It is more sophisticated and robust than the common used goodness of fit statistics, i.e. χ^2 prediction. For our sample, we find that fourth and third degree, $(J-K_{\mathrm{s}})_0$ only, polynomial fits represent the data best. Table 1 lists the corresponding coefficients and their errors. The fits together with the data are shown in Figure 3. All panels have the same scaling allowing to immediately compare the different plots. The

Table 1. The coefficients of the polynomial fits (Fig. 3) in the notation $\log T_{\rm eff} = {\rm a}_0 + {\rm a}_1({\rm color}) + {\rm a}_2({\rm color}^2)\ldots$ and the adjusted R-squared values.

	$(V-J)_0$	$(V-H)_0$	$(V-K_{\rm s})_0$	$(J-K_{\rm s})_0$
a_0	+4.002(1)	+3.992(1)	+4.000(1)	+4.006(3)
a_1	−0.425(6)	−0.339(4)	−0.328(4)	−1.320(22)
a_2	+0.462(13)	+0.301(8)	+0.282(6)	+2.58(22)
a_3	−0.353(37)	−0.180(18)	−0.171(14)	−1.88(59)
a_4	+0.099(36)	+0.040(9)	+0.039(7)	
R	0.989	0.989	0.992	0.939

$(J-K_{\rm s})_0$ calibration has a much more steeper gradient than the other three ones caused by the much narrower wavelength range covered. The calibrations are valid for $3.75 < \log T_{\rm eff} < 4.30$ dex and the following color range
$-0.42 < (V-J)_0 < +1.17$ mag
$-0.59 < (V-H)_0 < +1.48$ mag
$-0.54 < (V-K_{\rm s})_0 < +1.51$ mag
$-0.16 < (J-K_{\rm s})_0 < +0.38$ mag
The differences of the fit and the data show no systematical correlations over the complete color ranges. The 95% confidence bands for the calibrations are listed in Table 2. It gives the upper and lower limits for a given color value.

To get an estimate of the metallicity, i.e. [Fe/H] as an approximation, the database PAramètres STELlaires (PASTEL; Soubiran et al., 2010) was queried for entries of our sample stars. If more than one entry was found for an object, an unweighted mean was calculated. In total, [Fe/H] values for 67 stars ranging from −1.22 to +0.29 dex were found. For the projected rotational velocities ($v \sin i$), the starting point was the extensive catalog by Glebocki et al. (2000) which includes all published values until November 2000. We searched the literature for newer papers resulting in 27 additional publications used to derive mean values for 388 stars of our sample. The $v \sin i$ values range up to 343 km s^{-1}.

Figure 4 shows the differences of the effective temperature calibrations (Table 1) versus $v \sin i$ and [Fe/H] for the sample. There is a wide spread within the $v \sin i$ diagram visible, in particular for $(J-K_{\rm s})_0$. To test the symmetry around the zero value, a Wilcoxon sign rank and a Student's t-test (Hill & Lewicki, 2005) were used. The difference of both methods is that Wilcoxon sign rank test also accounts for a non-normal data distribution. None of these tests resulted in a deviation of symmetry with a significance of more than 5%. We can therefore conclude that, within the errors, the projected rotational velocity and metallicity does not affect the effective temperature calibrations.

Finally, the calibrations were checked with published intrinsic colors of dwarfs by Pecaut & Mamajek (2013). They used only spectral standard stars based on various publications from the literature. Also the effective temperatures were only taken from the literature. For their 30 listed values (Table 5 therein) within our investigated parameter range, the mean differ-

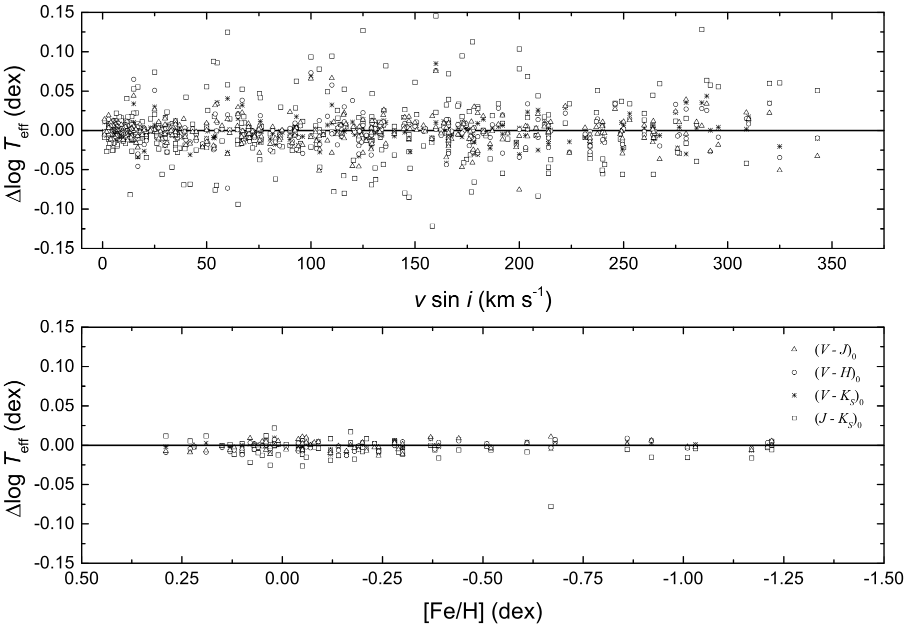

Fig. 4. The differences of the effective temperature calibrations (Table 1) versus $v \sin i$ and [Fe/H]. No systematics were detected.

ences of the calibrated $\log T_{\rm eff}$ values are below 0.004 dex with standard deviations between 0.007 and 0.014 dex, respectively. Wegner (2014) reported that the newly determined infrared intrinsic colors $(V-J)_0$, $(V-H)_0$, and $(V-K_{\rm s})_0$ differ significantly from those available in literature. However, comparing their values with those from Pecaut & Mamajek (2013), no statistically significant deviation from the one-to-one correlation is detected. The same is true for the comparison with our calibration.

The calibration was tested using two different group of stars and methods

- Niemczura et al. (2015) presented high-resolution spectroscopy of 117 A- and F-type ($3.83 < \log T_{\rm eff} < 4.03$ dex) stars from the Kepler field. They determined spectral types, atmospheric parameters (effective temperature, surface gravity, as well as microturbulent velocity), chemical abundances, and rotational velocities. We used their listed reddening estimates and the available $VJHK_{\rm s}$ photometry. The mean differences of the calibrated $\log T_{\rm eff}$ values in comparison with theirs are -0.005 dex with a standard deviation of 0.004 dex. This excellent agreement with spectroscopically determined effective temperatures provides confidence in our calibration.
- The chemically peculiar stars of the upper main sequence are characterized by peculiar and often variable line strengths, quadrature of line

variability with radial velocity changes, photometric variability with the same periodicity and coincidence of extrema (Bernhard et al., 2015). Slow rotation was inferred from the sharpness of spectral lines. Overabundances of several orders of magnitude compared to the Sun were derived for Silicon, Chromium, Strontium, and Europium, and for other heavy elements (Preston, 1974). The effective temperature of these objects was investigated by Netopil et al. (2008) using the Johnson UBV, Geneva 7-color, and, Strömgren-Crawford $uvby\beta$ photometric systems. In total, we compared the effective temperatures of 147 stars in common within the valid range of the calibration. The mean differences are $+0.007$ dex with a standard deviation of 0.006 dex over the complete spectral type range (B2 to F5).

These two examples show only a snapshot of the manifold applications for our calibration.

Conclusion

A new calibration of the effective temperature in terms of $VJHK_{\rm s}$ colors is presented. A homogeneous sample of main-sequence, B- to F-type stars with available high accurate photometric and astrometric data was build. Apparent variable, chemically peculiar, and binary stars were rejected. In total, 523 stars were found to meet our high standards.

The location of the targets within the HRD was established and checked for possible outliers. All objects lie, within the errors, between the ZAMS and TAMS, thus are hydrogen burning stars.

On the basis of precise Strömgren $uvby\beta$ photometry and its temperature calibration, correlations for $(V-J)_0$, $(V-H)_0$, $(V-K_{\rm s})_0$, and $(J-K_{\rm s})_0$ were derived. No dependency on the projected rotational velocity and metallicity was detected.

Tests with effective temperatures derived from high resolution spectroscopy and for chemically peculiar stars yielded an excellent agreement.

Acknowledgements

This project was supported by the grant GP14-26115P. This publication makes use of data products from the Two Micron All Sky Survey, which is a joint project of the University of Massachusetts and the Infrared Processing and Analysis Center/California Institute of Technology, funded by the National Aeronautics and Space Administration and the National Science Foundation.

References

Balona, L. A., 1994, *MNRAS*, 268, 119

Bernhard, K., Hümmerich, S., Paunzen, E., 2015, *Astronomische Nachrichten*, 336, 981

Breaz, N, 2004, *Acta Universitatis Apulensis, Mathematics-Informatics, număr dedicat Proc. of Int. Conf. on Theory and Appl. of Math. and Inf., Alba Iulia*, no. 7, Part B, p. 67

Bressan, A., Marigo, P., Girardi, L. et al., 2012, *MNRAS*, 427, 127

Buzzoni, A., Patelli, L., Bellazzini, M. et al., 2010, *MNRAS*, 403, 1592
Crawford, D. L., 1958, *ApJ*, 128, 185
Crawford, D. L., 1978, *AJ*, 83, 48
De Cat, P., Fu, J. N., Ren, A. B. et al., 2015, *ApJS*, 220, 19
di Benedetto, G. P., 1998, *A&A*, 339, 858
Domingo, A., Figueras, F., 1999, *A&A*, 343, 446
Dutra, C. M., Santiago, B. X., Bica, E., 2002, *A&A*, 381, 219
Fernley, J. A., 1989, *MNRAS*, 239, 905
Fiorucci, M., & Munari, U., 2003, *A&A*, 401, 781
Flower, P. J., 1996, *ApJ*, 469, 355
Francis, C., 2014, *MNRAS*, 444, L6
Garrison, R. F., Gray, R. O., 1994, *AJ*, 107, 1556
Geißler, K., Metchev, S., Kirkpatrick, J. D. et al., 2011, *ApJ*, 732, 56
Glebocki, R., Gnacinski, P., Stawikowski, A., 2000, *Acta Astron.*, 50, 509
Gonzalez, O. A., Rejkuba, M., Zoccali, M. et al., 2013, *A&A*, 552, A110
Hauck, B., Mermilliod, M., 1998, *A&AS*, 129, 431
Hertzsprung, E., 1911, *Publikationen des Astrophysikalischen Observatoriums zu Potsdam*, 22, A1
Hilditch, R. W., Hill, G., Barnes, J. V., 1983, *MNRAS*, 204, 241
Hill, T., Lewicki, P., 2005, *Statistics: Methods and Applications* (StatSoft, Inc.)
Holmberg, J., Nordström, B., Andersen, J., 2009, *A&A*, 501, 941
Houk, N., Swift, C., 1999, *Michigan catalogue of two-dimensional spectral types for the HD Stars*, Volume 5, Department of Astronomy, University of Michigan, Ann Arbor
Johnson, H. L., 1958, *Lowell Obs. Bull.*, 4, 37
Jordi, K., Grebel, E. K., Ammon, K., 2006, *A&A*, 460, 339
Kharchenko, N. V., 2001, *Kinematika i Fizika Nebesnykh Tel*, vol. 17, 409
Lawrence, A., Warren, S. J., Almaini, O. et al., 2007, *MNRAS*, 379, 1599
Lutz, T. E., Kelker, D. H., 1973, *PASP*, 85, 573
Masana, E., Jordi, C., Ribas, I., 2006, *A&A*, 450, 735
Morgan, W. W., Keenan, P. C., Kellman, E., 1943, *"An atlas of stellar spectra, with an outline of spectral classification"*, Chicago, Illinois, The University of Chicago press
Napiwotzki, R., Schoenberner, D., Wenske, V., 1993, *A&A*, 268, 653
Netopil, M., Paunzen, E., 2013, *A&A*, 557, A10
Netopil, M., Paunzen, E., Maitzen, H. M. et al., 2008, *A&A*, 491, 545
Niemczura, E., Murphy, S. J., Smalley, B. et al., 2015, *MNRAS*, 450, 2764
Paunzen, E., 1999, *A&A*, 341, 784
Paunzen, E., Schnell, A., Maitzen, H. M., 2005, *A&A*, 444, 941
Paunzen, E., Schnell, A., Maitzen, H. M., 2006, *A&A*, 458, 293
Pecaut, M. J., Mamajek, E. E., 2013, *ApJS*,, 208, 9
Perryman, M. A. C., 2005, in *ASP Conf. Ser. 338, Astrometry in the Age of the Next Generation of Large Telescopes*, ed. P. K. Seidelmann & A. K. B. Monet (San Francisco: ASP), 3
Perryman, M. A. C., Lindegren, L., Kovalevsky, J. et al., 1997, *A&A*, 323, L49
Pöhnl, H., Paunzen, E., 2010, *A&A*, 514, A81
Preston, G. W., 1974, *ARA&A*, 12, 257
Reis, W., Corradi, W., de Avillez, M. A. et al., 2011, *ApJ*, 734, 8
Renson, P., Manfroid, J., 2009, *A&A*, 498, 961
Robitaille, T. P., Whitney, B. A., Indebetouw, R. et al., 2007, *ApJS*, 169, 328
Russell, H. N., 1913, *The Observatory*, 36, 324
Samus, N. N., Durlevich, O. V., Kazarovets, E. V. et al., 2007 – 2016, *General Catalogue of Variable Stars*, VizieR On-line Catalog (http://cdsarc.u-strasbg.fr/viz-bin/Cat?B/gcvs)
Schlafly, E. F., Green, G., Finkbeiner, D. P. et al. 2014, *ApJ*, 789, 15
Schuster, W. J., Nissen, P. E., 1989, *A&A*, 221, 65
Skiff, B. A., 2009–2016, VizieR Online Data Catalog, 1
Skrutskie, M. F., Cutri, R. M., Stiening, R. et al., 2006, *AJ*, 131, 1163
Soubiran, C., Le Campion, J.-F., Cayrel de Strobel, G. et al., 2010, *A&A*, 515, A111
Strömgren, B., 1956, *Vistas in Astrononomy*, 2, 1336
Torres-Dodgen, A. V., Weaver, W. B., 1993, *PASP*, 105, 693
Tully, R. B., 2015, *AJ*, 149, 54
van Leeuwen, F., 2007, *A&A*, 474, 653
van Leeuwen, F., Fantino, E., 2005, *A&A*, 439, 791
Wegner, W., 2014, *Acta Astron.*, 64, 261
Worthey, G., Lee, H.-C., 2011, *ApJS*, 193, 1

Table 2. The 95% confidence bands of the calibrations (Fig. 3 and Table 1).

Color	$(V-J)_0$ $\log T_{\rm eff}$		$(V-H)_0$ $\log T_{\rm eff}$		$(V-K_{\rm s})_0$ $\log T_{\rm eff}$		$(J-K_{\rm s})_0$ $\log T_{\rm eff}$	
−0.58			4.328	4.333				
−0.56			4.310	4.315				
−0.54			4.293	4.298	4.287	4.291		
−0.52			4.276	4.281	4.271	4.275		
−0.50			4.260	4.265	4.256	4.260		
−0.48			4.244	4.249	4.241	4.245		
−0.46			4.229	4.234	4.227	4.231		
−0.44			4.214	4.219	4.213	4.216		
−0.42	4.289	4.294	4.200	4.205	4.199	4.203		
−0.40	4.269	4.274	4.186	4.191	4.186	4.190		
−0.38	4.249	4.254	4.173	4.178	4.173	4.177		
−0.36	4.231	4.235	4.160	4.165	4.161	4.165		
−0.34	4.213	4.218	4.148	4.152	4.149	4.153		
−0.32	4.196	4.200	4.136	4.140	4.138	4.141		
−0.30	4.179	4.184	4.124	4.128	4.127	4.130		
−0.28	4.163	4.168	4.113	4.117	4.116	4.119		
−0.26	4.148	4.153	4.102	4.106	4.106	4.109		
−0.24	4.134	4.138	4.092	4.096	4.095	4.099		
−0.22	4.120	4.124	4.082	4.085	4.086	4.089		
−0.20	4.107	4.111	4.072	4.076	4.076	4.080		
−0.18	4.094	4.098	4.062	4.066	4.067	4.071		
−0.16	4.081	4.085	4.053	4.057	4.059	4.062	4.285	4.298
−0.14	4.070	4.074	4.044	4.048	4.050	4.053	4.241	4.253
−0.12	4.059	4.062	4.036	4.039	4.042	4.045	4.199	4.211
−0.10	4.048	4.051	4.028	4.031	4.034	4.037	4.161	4.171
−0.08	4.037	4.041	4.020	4.023	4.026	4.029	4.124	4.134
−0.06	4.028	4.031	4.012	4.015	4.019	4.022	4.091	4.100
−0.04	4.018	4.022	4.005	4.008	4.012	4.015	4.059	4.068
−0.02	4.009	4.012	3.998	4.001	4.005	4.008	4.030	4.038
+0.00	4.000	4.004	3.991	3.994	3.998	4.001	4.003	4.010
+0.02	3.992	3.995	3.984	3.987	3.992	3.995	3.977	3.984
+0.04	3.984	3.987	3.978	3.981	3.986	3.988	3.954	3.961
+0.06	3.977	3.980	3.971	3.974	3.980	3.982	3.933	3.939
+0.08	3.969	3.972	3.965	3.968	3.974	3.976	3.913	3.919
+0.10	3.962	3.965	3.960	3.963	3.968	3.971	3.895	3.901
+0.12	3.956	3.959	3.954	3.957	3.963	3.965	3.879	3.885
+0.14	3.949	3.952	3.949	3.952	3.958	3.960	3.864	3.870
+0.16	3.943	3.946	3.944	3.946	3.953	3.955	3.850	3.856
+0.18	3.937	3.940	3.939	3.941	3.948	3.950	3.838	3.844
+0.20	3.932	3.934	3.934	3.936	3.943	3.945	3.827	3.834
+0.22	3.926	3.929	3.929	3.932	3.938	3.941	3.817	3.824
+0.24	3.921	3.924	3.925	3.927	3.934	3.936	3.808	3.816
+0.26	3.916	3.918	3.920	3.923	3.930	3.932	3.800	3.808
+0.28	3.911	3.914	3.916	3.919	3.925	3.928	3.793	3.802
+0.30	3.906	3.909	3.912	3.914	3.921	3.924	3.787	3.796
+0.32	3.902	3.904	3.908	3.910	3.917	3.920	3.782	3.791
+0.34	3.897	3.900	3.904	3.907	3.914	3.916	3.777	3.787
+0.36	3.893	3.895	3.900	3.903	3.910	3.912	3.772	3.783
+0.38	3.889	3.891	3.897	3.899	3.906	3.908	3.768	3.780
+0.40	3.885	3.887	3.893	3.896	3.903	3.905		
+0.42	3.881	3.883	3.890	3.892	3.899	3.901		
+0.44	3.877	3.880	3.886	3.889	3.896	3.898		
+0.46	3.873	3.876	3.883	3.885	3.893	3.895		
+0.48	3.870	3.872	3.880	3.882	3.889	3.892		
+0.50	3.866	3.869	3.877	3.879	3.886	3.888		
+0.52	3.863	3.865	3.874	3.876	3.883	3.885		
+0.54	3.859	3.862	3.871	3.873	3.880	3.882		
+0.56	3.856	3.858	3.868	3.870	3.877	3.879		
+0.58	3.852	3.855	3.865	3.867	3.874	3.877		
+0.60	3.849	3.851	3.862	3.865	3.872	3.874		
+0.62	3.845	3.848	3.859	3.862	3.869	3.871		
+0.64	3.842	3.845	3.857	3.859	3.866	3.868		
+0.66	3.839	3.842	3.854	3.857	3.863	3.865		
+0.68	3.836	3.838	3.851	3.854	3.861	3.863		
+0.70	3.832	3.835	3.849	3.851	3.858	3.860		
+0.72	3.829	3.832	3.846	3.849	3.855	3.858		
+0.74	3.826	3.829	3.844	3.846	3.853	3.855		
+0.76	3.823	3.826	3.841	3.844	3.850	3.852		
+0.78	3.819	3.822	3.839	3.841	3.848	3.850		
+0.80	3.816	3.819	3.836	3.839	3.845	3.847		
+0.82	3.813	3.816	3.834	3.837	3.843	3.845		
+0.84	3.810	3.813	3.831	3.834	3.840	3.843		
+0.86	3.806	3.810	3.829	3.832	3.838	3.840		
+0.88	3.803	3.806	3.827	3.829	3.835	3.838		
+0.90	3.800	3.803	3.824	3.827	3.833	3.835		
+0.92	3.796	3.800	3.822	3.825	3.830	3.833		
+0.94	3.793	3.797	3.819	3.822	3.828	3.830		
+0.96	3.790	3.794	3.817	3.820	3.825	3.828		
+0.98	3.786	3.790	3.814	3.818	3.823	3.826		
+1.00	3.783	3.787	3.812	3.815	3.821	3.823		
+1.02	3.780	3.784	3.810	3.813	3.818	3.821		
+1.04	3.776	3.781	3.807	3.811	3.816	3.818		
+1.06	3.773	3.777	3.805	3.808	3.813	3.816		
+1.08	3.770	3.774	3.802	3.806	3.811	3.814		
+1.10	3.766	3.771	3.800	3.803	3.808	3.811		
+1.12	3.763	3.768	3.797	3.801	3.806	3.809		
+1.14	3.760	3.764	3.795	3.799	3.804	3.806		
+1.16	3.757	3.761	3.793	3.796	3.801	3.804		
+1.18			3.790	3.794	3.799	3.802		
+1.20			3.788	3.792	3.796	3.799		
+1.22			3.785	3.789	3.794	3.797		
+1.24			3.783	3.787	3.791	3.795		
+1.26			3.780	3.784	3.789	3.792		
+1.28			3.778	3.782	3.787	3.790		
+1.30			3.775	3.779	3.784	3.787		
+1.32			3.773	3.777	3.782	3.785		
+1.34			3.770	3.775	3.779	3.783		
+1.36			3.768	3.772	3.777	3.780		
+1.38			3.765	3.770	3.775	3.778		
+1.40			3.763	3.767	3.772	3.776		
+1.42			3.760	3.765	3.770	3.773		
+1.44			3.758	3.763	3.768	3.771		
+1.46			3.756	3.760	3.765	3.769		
+1.48					3.763	3.767		
+1.50					3.761	3.765		